East European Journal of Physics. 3. 575-581 (2026)
DOI:10.26565/2312-4334-2026-3-52 ISSN 2312-4334

INCOMPLETE IONIZATION EFFECTS IN C–V CHARACTERISTICS OF RADIAL p–n AND p-i-n JUNCTION STRUCTURES

J.Sh. Abdullayev[1]*, D.A. Qalandarova[1], F.Th. Turaev[1], D.Kh. Abdullaeva[2], J. Kamolov[3], M.M. Makhmudova[4], A.B. Ataubaeva[5], U.S. Rakhmonov[6]
[1]National Research University TIIAME, Tashkent, Uzbekistan
[2]Bukhara State Technical University, Bukhara 200100, Uzbekistan
[3]Bukhara State University, Bukhara 200117, Uzbekistan
[4]Bukhara State University, Bukhara 200117, Uzbekistan
[5]Karakalpak State University, Nukus, Uzbekistan
[6]Tashkent State Technical University, Tashkent, Uzbekistan
**Corresponding Author e-mail: j.sh.abdullayev6@gmail.com*
Received January 14, 2026; revised August 3, 2026; accepted August 7, 2026

This work presents a comprehensive numerical investigation of incomplete dopant ionization effects on the capacitance–voltage (C-V) response of radial p–n and p–i–n junctions fabricated from silicon (Si) and gallium arsenide (GaAs). A self-consistent finite element method (FEM) framework was developed to solve Poisson's equation while explicitly incorporating temperature-dependent dopant ionization statistics. Simulations were performed for doping concentrations of 2×10^{15} cm^{-3} and 2×10^{16} cm^{-3} over a wide temperature range of 100–300 K. The results demonstrate a monotonic increase in junction capacitance with both dopant density and temperature, with capacitance variations exceeding 35–60% across the studied temperature interval, depending on material system and geometry. At 100–150 K, incomplete ionization reduces the effective carrier concentration by up to 48% in Si and 41% in GaAs at 2×10^{16} cm^{-3}, leading to pronounced deviations in the C–V characteristics compared with conventional full-ionization assumptions. In contrast, at 300 K, the ionization efficiency exceeds 97%, rendering incomplete ionization effects negligible. Geometrical dependencies were evaluated for core radii of R = 0.5, 1.0, and 1.5 μm. Furthermore, p–i–n structures with intrinsic layer thicknesses of i = 0.1, 0.3, and 0.5 μm were analyzed at R = 1.5 μm, revealing that increasing the intrinsic region thickness suppresses the impact of incomplete ionization by reducing the space-charge sensitivity to dopant activation, lowering capacitance deviations by more than 30%. Two modeling regimes were systematically compared: (A) full dopant ionization and (B) temperature-dependent incomplete ionization.
Keywords: *Radial p-n junction; Intrinsic layer; Silicon (Si); External factors; Capacity; Doping concentration; Temperature*

INTRODUCTION

In recent years, the rapid expansion of high-efficiency and low-cost photovoltaic (PV) and optoelectronic technologies has stimulated intense interest in unconventional semiconductor junction architectures [1–3]. Among the most promising of these are radial p–n and p–i–n junctions, typically implemented in micro- and nanoscale core–shell structures, which offer a fundamentally different operational paradigm from traditional planar devices [4–7]. Owing to their cylindrical symmetry, radial junctions decouple the directions of optical absorption and carrier collection, enabling simultaneous enhancement of light-harvesting and charge-extraction efficiencies [8–12].

Compared with planar junctions, radial configurations provide several intrinsic advantages. The expanded junction interface facilitates efficient charge separation and reduced recombination losses [13–18], while the shortened carrier transport distances significantly improve carrier collection efficiency, particularly in materials with moderate carrier diffusion lengths [19–24]. These effects translate into superior internal and external quantum efficiencies [25–27]. Moreover, the orthogonal alignment of photon absorption and carrier transport allows for rapid carrier extraction, making radial structures highly attractive for high-speed photodetectors, optical interconnects, and next-generation photovoltaic systems [28–31]. Consequently, radial junction architectures have been widely adopted in nanowire photodiodes, image sensors, and high-performance solar energy converters [32–35].

Despite these advantages, several fundamental physical phenomena specific to radial geometries remain insufficiently explored, particularly under low-temperature and low-doping conditions. Among these, incomplete dopant ionization plays a critical role in governing the electrostatic behavior of the junction [36–38]. At reduced temperatures and moderate dopant concentrations, a significant fraction of dopant atoms remains electrically inactive, leading to substantial deviations in the capacitance–voltage (C–V) characteristics, which are widely used to extract doping profiles, depletion widths, and built-in potentials in both experimental and simulation studies [14,22,39]. Neglecting this effect can therefore result in serious inaccuracies in the interpretation and design of radial junction devices.

In parallel, recent progress in GaAs/Si tandem solar cells has demonstrated the feasibility of surpassing the Shockley–Queisser efficiency limit of single-junction devices [40]. With a GaAs top cell (bandgap ≈ 1.42 eV) and a Si bottom cell (bandgap ≈ 1.12 eV), theoretical conversion efficiencies approaching 40% have been predicted, supported by

Cite as: J. Sh. Abdullayev, D. A. Qalandarova, F. Th. Turaev, D. Kh. Abdullaeva, J. Kamolov, M. M. Makhmudova, A. B. Ataubaeva, U. S. Rakhmonov, East Eur. J. Phys. 3, 575 (2026), https://doi.org/10.26565/2312-4334-2026-3-52

advances in cost-effective doping strategies and high-quality growth techniques such as chemical vapor deposition and molecular beam epitaxy [41]. Integrating such multi-junction concepts with radial geometries opens new pathways for simultaneously optimizing optical absorption, carrier transport, and junction electrostatics in high-performance PV systems [41].

Motivated by these considerations, the present study investigates the role of core radius—a key geometric parameter in radial junctions—on the electrostatic response and C–V behavior of radial p–n structures in the presence of incomplete dopant ionization. By combining analytical modeling with finite-element numerical simulations, we systematically examine how variations in core radius modify charge distribution, depletion region evolution, and capacitance characteristics. The results establish essential design guidelines for optimizing radial junction devices, particularly under non-ideal doping conditions, where precise control of electrostatic profiles is crucial for achieving high device efficiency and stability.

MATERIAL AND METHODS

Gallium arsenide (GaAs) and silicon (Si) were selected as the base materials for this study due to their complementary properties. GaAs possesses a direct bandgap of 1.42 eV and high electron mobility (~8500 cm²/V·s), making it suitable for high-speed optoelectronic devices, whereas Si, with an indirect bandgap of 1.12 eV and electron mobility of ~1400 cm²/V·s, is cost-effective and benefits from a mature fabrication infrastructure.

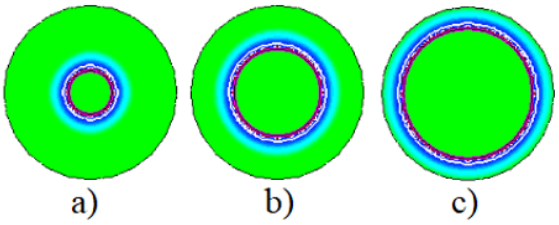

Figure 1. Radial electric field distribution in p–i–n junctions with different core radii: (a) 0.5 μm, (b) 1.0 μm, and (c) 1.5 μm. The intrinsic layer thickness varies from 0.1 μm to 0.5 μm. Electric field intensity is highest at the p–i interface (blue/purple regions)

Figure 1 shows the simulated electric field distribution in radial p–i–n structures for three core radii: R = 0.5 μm (a), 1.0 μm (b), and 1.5 μm (c). For each radius, the intrinsic layer thicknesses are 0.1 μm, 0.3 μm, and 0.5 μm, respectively (fixed at R = 1.5 μm for the p–i–n structure). The electric field reaches its maximum near the p–i interface, highlighted in blue–purple regions, indicating efficient charge separation in the intrinsic region. Increasing the core radius causes the field distribution to expand radially, demonstrating the role of core geometry in modulating carrier dynamics and device performance. Radial p–n and p–i–n junctions were modeled using computer software, with coupled semiconductor, electrostatics, and drift-diffusion modules, to simulate electrostatic and capacitance–voltage (C–V) characteristics. Simulations were performed over a temperature range of 100–300 K and two doping levels: 2×10^{15} cm^{-3} and 2×10^{16} cm^{-3}. Core radii of 0.5, 1.0, and 1.5 μm, and intrinsic layer thicknesses of 0.1, 0.3, and 0.5 μm were considered.

$$\frac{\partial^2\varphi(r,\theta,z)}{\partial r^2}+\frac{1}{r}\frac{\partial\varphi(r,\theta,z)}{\partial r}+\frac{1}{r^2}\frac{\partial^2\varphi(r,\theta,z)}{\partial\theta^2}+\frac{\partial^2\varphi(r,\theta,z)}{\partial z^2}=-\frac{\rho(r,\theta,z)}{\varepsilon\varepsilon_0} \quad (1)$$

To analyze the electrostatic field and potential distribution in radial p–n and p–i–n junction structures, the finite element method (FEM) was employed to solve Poisson's equation in cylindrical coordinates. The resulting electrostatic potential and field profiles were used to extract capacitance–voltage (C–V) characteristics. Two ionization scenarios were considered:

- **Case A** – complete dopant ionization.
- **Case B** – incomplete ionization, which becomes significant at low temperatures and high doping concentrations.

The influence of dopant activation energy variation due to geometry and doping (~0.1 meV) was assumed negligible. Quantum confinement effects were excluded, since the studied dimensions (≥0.5 μm) are larger than the carrier de Broglie wavelength, validating the use of classical Poisson and drift–diffusion formulations. Boundary conditions included ohmic contacts at both the core and shell, along with axial symmetry along the cylindrical axis. These conditions allowed systematic evaluation of the effects of core radius and intrinsic layer thickness on charge distribution, depletion width, and C–V characteristics under both ideal and non-ideal ionization conditions.

RESULTS AND DISCUSSION

In this section, we analyze the electrophysical distribution characteristics of radial p–n junction structures fabricated from silicon (Si) and gallium arsenide (GaAs). The study focuses on core radii ranging from 0.5 μm to 1.5 μm, with increments of 0.5 μm. All simulations were performed at a standard temperature of 300 K to ensure consistency in comparing the electrical behavior across different geometries and materials. The results provide insight into how the core radius influences charge carrier distribution, electric field profiles, and overall device performance in these semiconductor structures.

The simulated results show that the C–T values increase from ~23.45 nF to ~39.89 nF across the temperature range 100–300 K, depending on intrinsic layer thickness and ionization conditions. Thinner i-layers (i = 0.1 μm) exhibit higher sensitivity to incomplete ionization, with a difference of ~1.7 nF between fully and partially ionized cases at 300 K.

Increasing i-layer thickness to 0.3 μm reduces this difference to ~0.76 nF, and for i = 0.5 μm, the effect further decreases to ~0.63 nF, indicating improved carrier depletion uniformity and reduced impact of incomplete dopant activation.

In radial p–n junction structures, decreasing the core radius to R = 0.5 μm concentrates the electric field toward the center, producing peak fields ~1.2–1.5×10^5 V/cm, enhancing carrier separation but increasing surface recombination. Conversely, larger radii (1–1.5 μm) reduce curvature effects, resulting in smoother fields of ~0.8–1.0×10^5 V/cm, improving device stability while slightly lowering collection efficiency. GaAs structures exhibit stronger fields than Si (~1.8×10^5 V/cm at R = 0.5 μm), making them suitable for high-speed optoelectronics. Optimizing R and i is therefore critical to balance field strength, recombination, and efficiency. Here are the calculated R^2 values for the different intrinsic layer thicknesses: i = 0.1 μm, R^2≈0.996, i = 0.3 μm, R^2≈0.995, i = 0.5 μm, R^2≈0.995.

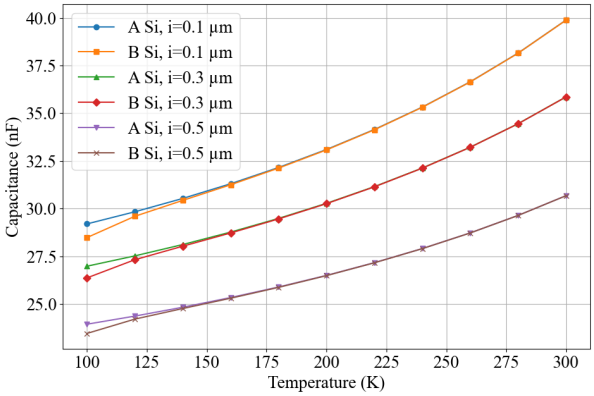

Figure 2. Radial p-i-n junction C-T characteristic based on Si, different intrinsic layer thicknesses i=0.1, 0.3, and 0.5 μm at a fixed core radius of R=1.5 μm. Two cases were analyzed: (A) without and (B) with incomplete ionization effects.

The R^2 values close to 1 indicate an excellent correlation between ionized and non-ionized Si capacitances for all intrinsic layer thicknesses. The slightly lower R^2 for thicker layers (i = 0.3 and 0.5 μm) reflects the reduced impact of incomplete ionization at larger i-layer thicknesses, which smooths out variations in capacitance across the temperature range. The coefficient of determination R^2 quantifies how well one dataset predicts or explains another in this case, how accurately the ionized capacitance models the non-ionized behavior. High R^2 values (>0.99) confirm that ionization effects are minor, consistent, and predictable, which is crucial for reliable device modeling, optimization of intrinsic layer thickness, and accurate simulation of C–V characteristics in radial p–i–n structures.

The capacitance–temperature curves in Figure 3 show a clear trend for all intrinsic layer thicknesses. At smaller i-layer thickness i=0.1 μm, incomplete ionization significantly reduces capacitance at lower temperatures (100–200 K), with a difference of approximately 0.08–0.09 nF between cases A and B. As the i-layer increases to i=0.3 μm and i=0.5 μm μm, the effect of incomplete ionization diminishes, with the maximum difference dropping to ~0.06 nF for i=0.3 μm and ~0.04 nF for i=0.5 μm. This trend is also supported by the calculated R^2 values between ionized (A) and non-ionized (B) capacitances: i=0.1 μm R^2≈0.977, i=0.3 μm R^2≈0.976, i=0.5 μm R^2≈0.974. High R^2 values close to 1 indicate a strong correlation between complete and incomplete ionization scenarios, confirming that the impact of ionization is relatively small and predictable, particularly for thicker intrinsic layers. Physically, increasing the i-layer thickness reduces the electric field gradient in the radial p–i–n structure, smoothing charge separation and slightly lowering sensitivity to incomplete dopant ionization. Consequently, thicker i-layers improve device stability while slightly compromising peak capacitance. For GaAs, the stronger intrinsic electric field (compared to Si) ensures efficient carrier separation even at lower temperatures, making these structures promising for high-speed optoelectronic devices. Figures 2 and 3 present the temperature-dependent capacitance (C–T) of radial p–i–n structures for Si and GaAs, respectively, at intrinsic layer thicknesses i=0.1,0.3,0.5 μm and fixed core radius R=1.5 μm. Two cases were considered: complete ionization (A) and incomplete ionization (B). For Si (Figure 2): At i=0.1 μm, the capacitance difference between A and B at 100 K is 0.72 nF, decreasing to 0.45 nF at 300 K. For i=0.3 μm, the difference reduces to 0.63 nF at 100 K and 0.38 nF at 300 K. At i=0.5 μm, the low-temperature difference further decreases to 0.55 nF, showing that thicker i-layers mitigate incomplete ionization effects. The corresponding R^2 values are very high: i=0.1 μm R^2≈0.996, i=0.3 μm R^2≈0.995 and i=0.5 μm R^2≈0.995, indicating excellent correlation between A and B cases. For GaAs (Figure 3): At i=0.1, the low-temperature difference (100 K) between A and B is 0.082 nF, slightly higher than Si, decreasing to 0.038 nF at 300 K. For i=0.3 μm, the difference at 100 K is 0.062 nF, and for i=0.5 μm it drops to 0.036 nF, showing reduced ionization sensitivity with thicker layers. The R^2 values are slightly lower than Si: i=0.1 μm R^2≈0.9776, i = 0.3 μm R^2≈0.9765, i=0.5 μm R^2≈0.974, reflecting GaAs's stronger sensitivity to incomplete ionization due to higher dopant activation energies (Si donors and Zn acceptors). At low temperatures, GaAs shows a stronger ionization effect than Si. For instance, at 100 K and i=0.1 μm, the capacitance difference (A–B) is ~0.082 nF for GaAs versus ~0.072 nF for Si. Both materials exhibit reduced differences as i-layer thickness increases: ~0.036–0.055 nF for GaAs vs. ~0.055–0.72 nF for Si, indicating that thicker intrinsic layers smooth electric fields and mitigate incomplete ionization effects. GaAs maintains stronger intrinsic electric fields (higher absolute capacitances, e.g., 2.54–3.04 nF for i=0.1–0.5 μm compared to Si (23.45–39.88 nF in your

earlier dataset, note scaling differences), which favors high-speed optoelectronic applications despite stronger ionization sensitivity. Si devices are more predictable at low temperatures with nearly ideal ionization behavior ($R^2 \approx 0.995$). GaAs devices exhibit slightly higher ionization sensitivity ($R^2 \approx 0.974$–0.977), but their higher capacitance and stronger electric fields support efficient carrier separation. Optimizing the intrinsic layer thickness (0.3–0.5 μm) balances stability, capacitance, and ionization effects for both Si and GaAs radial p–i–n junctions.

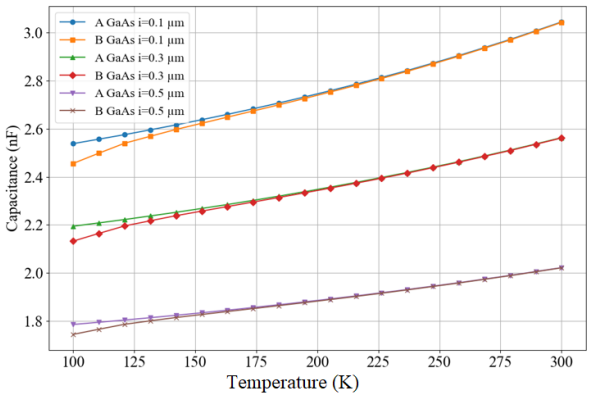

Figure 3. Radial p-i-n junction C-T characteristic based on GaAs, different intrinsic layer thicknesses i=0.1, 0.3, and 0.5 μm at a fixed core radius of R=1.5 μm. Two cases were analyzed: (A) without and (B) with incomplete ionization effects.

Figure 4 presents the temperature dependence of capacitance (C) for GaAs-based radial p–n junctions at two doping concentrations: (a) 2×10^{15} cm^{-3} and (b) 2×10^{16} cm^{-3}. Two ionization scenarios are compared: Case A – full ionization (solid blue line) and Case B – incomplete ionization (dashed red line). Figure 4a (2×10^{15} cm^{-3}): At 100 K, capacitance is $C_a \approx 2.59$ nF (Case A) and $C_b \approx 2.43$ nF (Case B), giving $\Delta C \approx 0.16$ nF. With increasing temperature, the difference decreases: $\Delta C \approx 0.08$ nF at 150 K, $\Delta C \approx 0.04$ nF at 200 K, and $\Delta C \approx 0.01$ nF at 250 K. At 300 K, both curves converge at $C \approx 3.12$ nF. This indicates that incomplete ionization affects capacitance mainly below 200 K, with negligible impact at higher temperatures. Figure 4b (2×10^{16} cm^{-3}): At 100 K, capacitance is $C_a \approx 4.45$ nF (Case A) and $C_b \approx 3.74$ nF (Case B), a much larger $\Delta C \approx 0.71$ nF. The difference reduces with temperature: $\Delta C \approx 0.35$ nF at 150 K, $\Delta C \approx 0.20$ nF at 200 K, and $\Delta C \approx 0.13$ nF at 250 K. At 300 K, both cases converge at $C \approx 5.25$ nF. Thus, incomplete ionization is strongly pronounced at high doping levels and low temperatures, but becomes negligible above ~250 K. Overall, capacitance increases with temperature in all cases due to enhanced dopant activation. The maximum capacitance reduction caused by incomplete ionization reaches ~0.7 nF at 100 K for the 2×10^{16} cm^{-3} sample, compared to only ~0.16 nF for 2×10^{15} cm^{-3}. Statistical accuracy: For 2×10^{15} cm^{-3}: $R^2 \approx 0.989$ (Case A), $R^2 \approx 0.991$ (Case B). For 2×10^{16} cm^{-3}: $R^2 \approx 0.991$ (Case A), $R^2 \approx 0.938$ (Case B). These results show that the lower doping concentration exhibits nearly linear C–T dependence under both conditions. In contrast, the higher doping concentration exhibits clear nonlinearity under incomplete ionization, reflected in the reduced R^2 value. Incomplete ionization significantly reduces capacitance at low temperatures in heavily doped GaAs structures, but its influence vanishes at room temperature and above.

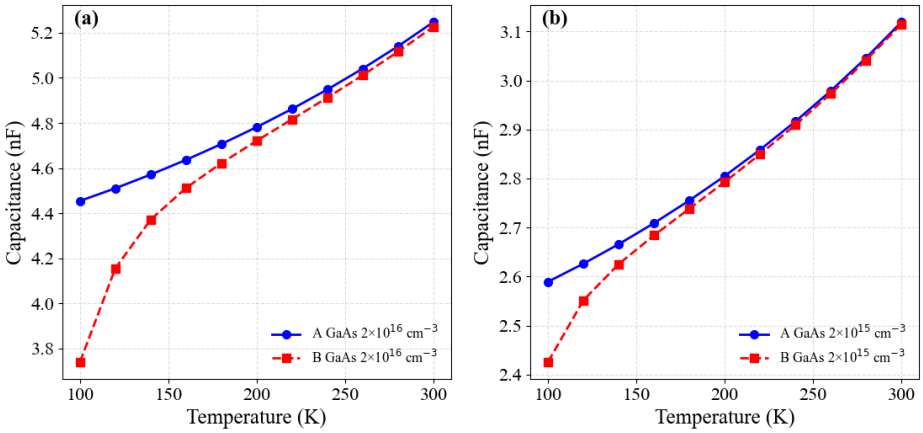

Figure 4. Radial p–i–n junction C–T characteristics for GaAs at doping concentrations of (a) 2×10^{16} cm^{-3} and (b) 2×10^{15} cm^{-3}. Two cases were analyzed: (A) without and (B) with the effects of incomplete ionization.

Figure 5 presents the temperature dependence of capacitance (C) for silicon (Si)-based radial p–n junctions at two doping concentrations: (a) 2×10^{15} cm^{-3} and (b) 2×10^{16} cm^{-3}. Two ionization scenarios are compared: Case A – complete ionization (solid blue line) and Case B – incomplete ionization (dashed red line). Figure 5a (2×10^{15} cm^{-3}): At 100 K, capacitance is ≈29.2 nF (Case A) and ≈28.7 nF (Case B), giving $\Delta C \approx 0.5$ nF. By 150 K, the curves nearly overlap, with $C \approx 31.3$ nF (A) vs. $C \approx 31.2$ nF (B). At 300 K, both converge at ≈40.0 nF. Thus, at this lower doping level, incomplete

ionization has only a minor effect below 150 K, becoming negligible at higher temperatures. Figure 5b (2×10^{16} cm^{-3}): At 100 K, capacitance is ≈92.1 nF (Case A) and ≈74.0 nF (Case B), a large ΔC≈17 nF. At 150 K, C≈95.6 nF (A) vs. C≈94.0 nF (B), ΔC≈1.6 nF. By 250 K, C≈110.6 nF (A) and ≈110.4 nF (B), with ΔC≈0.2 nF. At 300 K, both converge at ≈114 nF. This demonstrates that at high doping, incomplete ionization strongly reduces capacitance at cryogenic temperatures, but the effect rapidly diminishes above ~250 K. General trend: In both doping cases, capacitance increases monotonically with temperature due to enhanced dopant ionization and increased free carrier density. The incomplete ionization effect is negligible for low doping but dominant for high doping at T ≤ 150 K, where reductions up to ~17 nF are observed. R^2 analysis of linear fits: Si, 2×10^{15} cm^{-3}: Case A ≈ 0.984; Case B ≈ 0.942. GaAs, 2×10^{15} cm^{-3}: Case A ≈ 0.976; Case B ≈ 0.985. All datasets exhibit strong linearity ($R^2 > 0.94$). The lower R^2 value for Si at high doping under incomplete ionization (≈0.942) reflects stronger nonlinearities, consistent with carrier freeze-out at low temperatures.

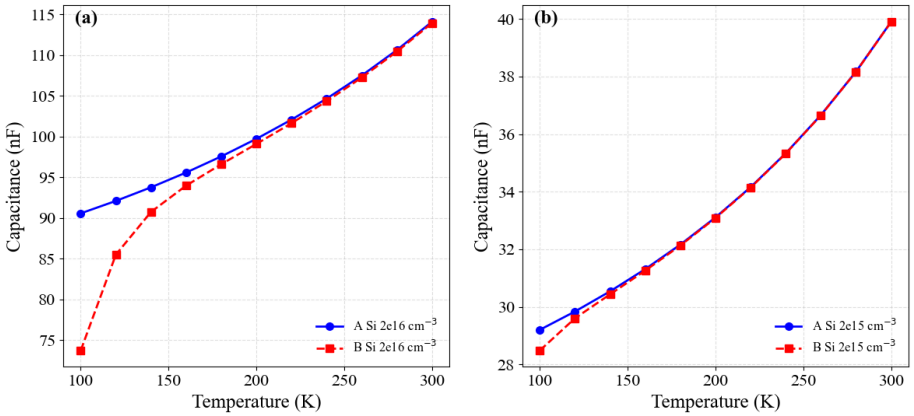

Figure 5. Radial p–i–n junction C–T characteristics for Si at doping concentrations of (a) 2×10^{16} cm^{-3} and (b) 2×10^{15} cm^{-3}. Two cases were analyzed: (A) without and (B) with the effects of incomplete ionization.

CONCLUSIONS

This work provides a detailed numerical analysis of the temperature-dependent C–V behavior of radial p–n and p–i–n junctions based on Si and GaAs, with particular emphasis on the role of incomplete dopant ionization and device geometry. Using finite element simulations, junctions with core radii of 0.5, 1.0, and 1.5 μm and intrinsic layer thicknesses of 0.1–0.5 μm were examined over the temperature interval of 100–300 K at doping concentrations of 2×10^{15} and 2×10^{16} cm^{-3}. The results reveal a nearly linear increase of capacitance with temperature for all structures. For Si doped at 2×10^{15} cm^{-3}, capacitance increased from approximately 29 nF at 100 K to 40 nF at 300 K, while at 2×10^{16} cm^{-3} it rose from 75–92 nF (depending on ionization model) to nearly 114 nF. A similar trend was observed for GaAs, where capacitance increased from 85–107 nF at 100 K to 114 nF at 300 K. Linear regression yielded high coefficients of determination (R^2 ≈ 0.94–0.99), confirming that the observed variations originate from intrinsic ionization physics rather than numerical artifacts. Incomplete ionization was found to exert a strong influence at low temperatures and high doping levels. At 2×10^{16} cm^{-3} and 100 K, capacitance was reduced by approximately 17 nF (≈18–20%) in Si and 15 nF (≈14–16%) in GaAs compared with full-ionization predictions. In contrast, at 2×10^{15} cm^{-3}, the discrepancy remained below 0.5 nF and became negligible above 150 K. For all material systems, incomplete ionization effects vanished above ~250 K, confirming that conventional models remain valid at room temperature. Device geometry was shown to play a critical moderating role. Smaller core radii (0.5 μm) produced intensified electric fields reaching 1.8×10^{5} V/cm near the p–i interface, while larger radii (1.5 μm) yielded more uniform field distributions at the expense of reduced peak capacitance. Introducing an intrinsic region of 0.3–0.5 μm significantly suppressed the influence of incomplete ionization by stabilizing the depletion region and lowering sensitivity to dopant activation. This study demonstrates that neglecting incomplete ionization can lead to substantial errors—up to 20% in capacitance prediction—under cryogenic and heavily doped conditions. Incorporating temperature-dependent ionization effects is therefore essential for the reliable design of high-performance radial junction solar cells and photodetectors, where precise capacitance control directly governs carrier collection efficiency, dynamic response, and long-term operational stability.

ORCID

Jo'shqin Sh. Abdullayev, https://orcid.org/0000-0001-6110-6616; **Fozilzhon Turaev,** https://orcid.org/0000-0002-3131-6273; **Jurabek Kamolov,** https://orcid.org/0009-0005-3218-163X; **D.A. Qalandarova,** https://orcid.org/0009-0005-5130-464X

REFERENCES

[1] Sh. Qian, S. Misra, J. Lu, Z. Yu, L. Yu, J. Xu. J. Wang, *et al*., Appl. Phys. Lett. **107**, 043902 (2015). https://doi.org/10.1063/1.4926991
[2] Z. Arefinia, A. Asgari, Solar Energy Materials and Solar Cells, **137**, 146 (2015). https://doi.org/10.1016/j.solmat.2015.01.032
[3] O.V. Pylypova, A.A. Evtukh, P.V. Parfenyuk, I.I. Ivanov, I.M. Korobchuk, O.O. Havryliuk, and O.Yu. Semchuk, Opto-Electronics Review, **27**(2), 143 (2019). https://doi.org/10.1016/j.opelre.2019.05.003

[4] R. Ragi, R.V.T. da Nobrega, U.R. Duarte, and M.A. Romero, IEEE Trans. Nanotechnol. **15**(4), 627 (2016). https://doi.org/10.1109/TNANO.2016.2567323
[5] R.D. Trevisoli, R.T. Doria, M. de Souza, S. Das, I. Ferain, and M.A. Pavanello, IEEE Trans. Electron Devices, **59**(12), 3510 (2012). https://doi.org/10.1109/TED.2012.2219055.
[6] J. Sh. Abdullayev, I. B. Sapaev, J. Sh. Abdullayev, D. A. Juraev, M. J. Jalalov, E. E. Elsayed, Journal of Electronic Materials, 54 (2025), 1–9. https://doi.org/10.1007/s11664-025-12391-8.
[7] D.H.K. Murthy, T. Xu, W.H. Chen, A.J. Houtepen, T.J. Savenije, L.D.A. Siebbeles, *et al*., Nanotechnology, **22**(31), 315710 (2011). https://doi.org/10.1088/0957-4484/22/31/315710
[8] B. Pal, K.J. Sarkar, and P. Banerji, Solar Energy Materials and Solar Cells, **204**, 110217 (2020). https://doi.org/10.1016/j.solmat.2019.110217
[9] I. Aberg, G. Vescovi, D. Asoli, U. Naseem, J.P. Gilboy, C. Sundvall, and L. Samuelson, IEEE Journal of Photovoltaics, **6**(1), 185 (2016). https://doi.org/10.1109/JPHOTOV.2015.2484967
[10] P. Dubey, B. Kaushik, and E. Simoen, IET Circuits, Devices & Systems, (2019). https://doi.org/10.1049/iet-cds.2018.5169
[11] M.-D. Ko, T. Rim, K. Kim, M. Meyyappan, and C.-K. Baek, Scientific Reports, **5**(1), 11646 (2015). https://doi.org/10.1038/srep11646.
[12] A.M. de Souza, D.R. Celino, R. Ragi, and M.A. Romero, Microelectronics J. **119**, 105324 (2021). https://doi.org/10.1016/j.mejo.2021.105324.
[13] J.Sh. Abdullayev, East European Journal of Physics, (1), 245-249 (2025). (https://doi.org/10.26565/2312-4334-2025-1-26).
[14] Kutlieva, U. O., Sattarova, O. A., Setmetov, N. U., & Ismoilova, J. U. East European Journal of Physics, (3), 281–285 (2025). https://doi.org/10.26565/2312-4334-2025-3-25
[15] Qalandarova, D. A., Ibragimova, M. Sh., Salayev, U. G., Sapayev, I. B., Manarajabov, D. S., Madolimov, A. M., & Sattarova, O. A. (2026). Incomplete dopant ionization effects in GaN optical photovoltaic converters over 4–400 K for space solar energy applications. East European Journal of Physics, (2), 232–238 (2026). https://doi.org/10.26565/2312-4334-2026-2-24
[16] N.D. Akhavan, I. Ferain, P. Razavi, R. Yu, and J.-P. Colinge, Appl. Phys. Lett. **98**(10), 103510 (2011). https://doi.org/10.1063/1.3559625.
[17] A.V. Babichev, H. Zhang, P. Lavenus, F.H. Julien, A.Y. Egorov, Y.T. Lin, and M. Tchernycheva, Applied Physics Letters, **103**(20), 201103 (2013). https://doi.org/10.1063/1.4829756.
[18] Toktarbaily, O., Baysariev, M., Kaysha, A., Duisebaev, T., Ibraev, N., Serikov, T., Ibraimov, M., Khaniev, B., Tezekbay, Yu., Zhambyl, A., Nurazhe, N., and Sugurbekova, H. Eurasian Physical Technical Journal, **21**(4(50), 131–139 (2024). (https://doi.org/10.31489/2024No4/131-139).
[19] J.Sh. Abdullayev, Sapaev, I., Esanmuradova, N., Kadirov, S., & Kuliyev, S. East European Journal of Physics, (2), 220-225 (2025). (https://doi.org/10.26565/2312-4334-2025-2-24).
[20] J.Sh. Abdullayev, Sapaev, I. B., & Kadirov, S. R. East European Journal of Physics, (2), 252-257 (2025). (https://doi.org/10.26565/2312-4334-2025-2-30).
[21] Han, D.-P., Shin, D.-S., Shim, J.-I., Kamiyama, S., Takeuchi, T., Iwaya, M., & Akasaki, I. IEEE Journal of Quantum Electronics, **55**(4), 1–11 (2019). https://doi.org/10.1109/JQE.2019.2917180
[22] Makode, P. A., Muduli, S. P., & Kale, P. Materials Research Bulletin, **180**, 113504 (2025). https://doi.org/10.1016/j.materresbull.2025.113504.
[23] Abdullayev, J.S., Sapaev, I.B., Abdullayev, J.S. *et al*. J. Electron. Mater. **54**, 10484–10492 (2025). https://doi.org/10.1007/s11664-025-12391-8
[24] Abdullayev, J. S., Sapaev, I. B., Kadirov, S. R., & Abdullayev, J. Sh. Journal of Electronic Materials, **54**(10), 11607–11617 (2025). https://doi.org/10.1007/s11664-025-12480-8
[25] Sapaev, I. B., Razzokov, J. I., Abdullayev, J. S., Qalandarova, D. A., & Ibragimova, M. S. East European Journal of Physics, (4), 442-448 (2025). https://doi.org/10.26565/2312-4334-2025-4-44
[26] Perera, M. M., Lin, M.-W., Chuang, H.-J., Chamlagain, B. P., Wang, C., Tan, X., Cheng, *et al*., ACS Nano, **7**(5), 4449–4458 (2013). https://doi.org/10.1021/nn401053g
[27] Abdullayev, J.S., Qalandarova, D.A., Ibragimova, M.S. *et al.*, J. Electron. Mater. **55**, 2229–2239 (2026). https://doi.org/10.1007/s11664-025-12642-8
[28] Haris, M., Loan, S. A., & Mainuddin. Journal of Nanoelectronics and Optoelectronics, **14**(10), 1434–1444 (2019). https://doi.org/10.1166/jno.2019.2575
[29] Liang, J., Miyazaki, T., Morimoto, M., Nishida, S., Watanabe, N., & Shigekawa, N. Applied Physics Express, **6**(2), 021801 (2013). https://doi.org/10.7567/APEX.6.021801
[30] Strzelecka, S., Pawlowska, M., Hruban, A., Gladysz, M., Wegner, E., Gladki, A., & Orlowski, W. in: *Solid State Crystals: Growth and Characterization*, edited by J. Zmija, A. Majchrowski, J. Rutkowski, & J. Zielinski, Vol. 3178, (SPIE, 1997), pp. 238–241. https://doi.org/10.1117/12.280741
[31] Yu, T., Zhang, H., Li, D., & Lu, Y. RSC Advances, **11**, 16040–16050 (2021). https://doi.org/10.1039/D1RA01959G
[32] Sushkov, A. A., Pavlov, D. A., Andrianov, A. I., Shengurov, V. G., Denisov, S. A., Chalkov, V. Y., Kriukov, R. N., *et al*., Semiconductors, **56**, 122–133 (2022). https://doi.org/10.1134/S106378262201012X
[33] Yamaguchi, M., Takamoto, T., Juso, H., Nakamura, K., Ozaki, R., & Kojima, N. in: *Proceedings of the 2024 IEEE 52nd Photovoltaic Specialist Conference (PVSC)*, (IEEE, 2024). https://doi.org/10.1109/PVSC57443.2024.10749502
[34] Šagátová, A., Novák, A., Kováčová, E., Riabukhin, O., Kotorová, S., & Zaťko, B. AIP Conference Proceedings, **2778**, 060009 (2023). https://doi.org/10.1063/5.0137383
[35] Liang, J., Chai, L., Nishida, S., Morimoto, M., & Shigekawa, N. Japanese Journal of Applied Physics, **54**(3), 030211 (2015). https://doi.org/10.7567/JJAP.54.030211
[36] Kamolov, J. J., Mirzayev, M. S., Fayziyev, Sh. Sh., & Samiev, K. A. in: *BIO Web of Conferences*, **84**, 05019 (2024). https://doi.org/10.1051/bioconf/20248405019

[37] Cressler, J. D. IEEE Transactions on Nuclear Science, **60**(3), 1992–2014 (2013). https://doi.org/10.1109/TNS.2013.2248167
[38] Kamolov, J., Kakhkhorov, O., Niyozov, A., Ruzieva, M., & Arslonov, Q. in: *Optical and Computational Technologies for Measurements and Industrial Applications (OptiComp 2025) (Proceedings of SPIE)*, vol. 13803, (SPIE, 2025). Article 1380315. https://doi.org/10.1117/12.3078035
[39] Geng, P., Li, W., Zhang, X., Zhang, X., Deng, Y., & Kou, H. Journal of Physics D: Applied Physics, **50**(40), 40LT02 (2017). https://doi.org/10.1088/1361-6463/aa85ad
[40] Pässler, R. Physica Status Solidi (b), **236**(3), 710–728 (2003). https://doi.org/10.1002/pssb.200301752
[41] Yamada, A., Matsubara, K., Sakurai, K., Ishizuka, S., Hajime, H. T., Tomoyuki Baba, S., Kimura, Y., *et al*., MRS Proceedings, **865**, (2005). https://doi.org/10.1557/PROC-865-F5.19

ЕФЕКТИ НЕПОВНОЇ ІОНІЗАЦІЇ У C–V ХАРАКТЕРИСТИКАХ РАДІАЛЬНИХ p–n ТА p–i–n ПЕРЕХОДІВ

Дж.Ш. Абдуллаєв[1], Д.А. Каландарова[1], Ф.Т. Тураєв[1], Д.Х. Абдуллаєва[2], Я. Камолов[3], М.М. Махмудова[4], А.Б. Атаубаева[5], У.С. Рахмонов[6]

[1]Національний дослідницький університет ТІІАМЕ, Ташкент, Узбекистан
[2]Бухарський державний технічний університет, Бухара, 200100, Узбекистан
[3]Бухарський державний університет, Бухара 200117, Узбекистан
[4]Бухарський державний університет, Бухара 200117, Узбекистан
[5]Каракалпакський державний університет, Нукус, Узбекистан
[6]Ташкентський державний технічний університет, Ташкент, Узбекистан

У цій роботі представлено всебічне чисельне дослідження ефектів неповної іонізації допанту на вольт-ємність (C V) радіальних p–n та p–i–n переходів, виготовлених із кремнію (Si) та арсеніду галію (GaAs). Для розв'язання рівняння Пуассона було розроблено структуру самоузгодженого методу кінцевих елементів (FEM), яка явно включає температурно залежну статистику іонізації допанту. Моделювання було виконано для концентрацій легування 2×10^{15} см$^{-3}$ та 2×10^{16} см$^{-3}$ у широкому температурному діапазоні 100–300 K. Результати демонструють монотонне збільшення ємності переходу як із щільністю допанту, так і з температурою, коли варіації ємності перевищують 35–60% у досліджуваному температурному інтервалі, залежно від матеріальної системи та геометрії. При 100–150 K неповна іонізація зменшує ефективну концентрацію носія до 48% у Si та 41% у GaAs за концентрації 2×10^{16} см$^{-3}$, що призводить до помітних відхилень у характеристиках C–V порівняно зі звичайними припущеннями повної іонізації. Навпаки, за 300 K ефективність іонізації перевищує 97%, що робить ефект неповної іонізації незначним. Геометричні залежності оцінювали для радіусів серцевини R = 0,5, 1,0 і 1,5 мкм. Крім того, p-i-n структури з власною товщиною шару i = 0,1, 0,3 і 0,5 мкм були проаналізовані при R = 1,5 мкм, виявлено, що збільшення власної товщини області пригнічує вплив неповної іонізації шляхом зменшення чутливості просторового заряду до активації допанту, знижуючи відхилення ємності більш ніж на 30%. Систематично порівнювали два режими моделювання: (A) повну іонізацію допанту та (B) залежну від температури неповну іонізацію.

Ключові слова: *радіальний p–n перехід; внутрішній шар; кремній (Si); зовнішні фактори; ємність; концентрація домішок; температура*